ADVANCED FUNCTIONAL MATERIALS

DOI: 10.1002/adfm.200800206

Lattice-Registered Two-Photon Polymerized Features within Colloidal Photonic Crystals and Their Optical Properties**

By *Erik C. Nelson, Florencio García-Santamaría,* and *Paul V. Braun**

In this work we demonstrate a significant advance in the introduction of embedded defects in 3D photonic crystals by means of two-photon polymerization. We have developed the ability to precisely position embedded defects with respect to the lattice of 3D photonic crystals by imaging the structure concurrently with two-photon writing. Defects are written with near-perfect lattice registration and at specifically defined depths within the crystal. The effect of precise defect position on the optical response is investigated for embedded planar cavities written in a photonic crystal. The experimental data are compared to spectra calculated using the Scalar Wave Approximation (SWA).

1. Introduction

Photonic crystals (PhCs) are structures having a periodic modulation of their dielectric constant on length scales comparable to the wavelength of light they are designed to manipulate. For certain 3D structures of sufficiently high dielectric contrast, a photonic bandgap (PBG) may result, preventing propagation of certain frequencies of light within the crystal.[1–3] The introduction of controllably positioned predesigned defects (e.g., optical cavities) in these PBG materials[4] is in anology with doping semiconductors and enables many potential applications, such as optical circuits,[5–7] low-loss waveguides,[3,8] and low-threshold lasers.[1]

We have previously shown that two-photon polymerization (TPP) allows for the controlled addition of high resolution defects into a 3D self-assembled colloidal crystal.[9,10] However, due to the low resolution of the reflectance imaging procedure employed during the TPP writing, previous results only showed a limited degree of control on the registration of the embedded features with respect to the surrounding lattice. The alignment was insufficient to satisfy the demanding requisites of a number of optically functional structures.[11–14] For example, the confinement power (Q-factor) and resonant frequency of certain cavities within 3D PhCs have been shown to be a function of defect position within the photonic crystal lattice.[13] An advantage of being able to precisely position point defects is that it becomes possible to fabricate low-loss waveguides in colloidal crystals[12] and to improve the coupling efficiency between a cavity and a waveguide or a second cavity.[14] Furthermore, obtaining high quality images of the colloidal crystal during the TPP would permit avoiding writing the features in areas where defects inherent to the self-assembly process (e.g., vacancies, cracks, and stacking faults) are present. Such unwanted defects degrade the optical properties of the system and their presence has not yet been completely eliminated despite the fact that the density of unwanted defects in colloidal crystals has been reduced substantially in the past few years.[15,16]

Here we demonstrate the ability to write embedded features with excellent lattice registration and placement with respect to unwanted crystalline defects by switching from a reflective to a fluorescent imaging technique. Planar cavities, 3D features and point defects are obtained using the new procedure. Spectroscopy performed on samples with planar cavities and the modeling of the results confirm that the position of the cavity with respect to the crystal significantly affects the optical response.

2. Reflectance versus Fluorescence Imaging

Reflectance confocal imaging relies on reflections from interfaces to construct an image. By necessity for TPP, the monomer is nearly index matched to the colloids to minimize light scattering during writing, therefore reflections from the monomer/colloid interface are low, reducing the resolution of the reflectance image. Concurrent high resolution imaging and feature writing can be achieved by introducing a boron

[*] Prof. P. V. Braun, E. C. Nelson, Dr. F. García-Santamaría[+]
Department of Materials Science and Engineering
Beckman Institute
1304 West Green St., Urbana, IL 61801 (USA)
E-mail: pbraun@illinois.edu
Prof. P. V. Braun, E. C. Nelson, Dr. F. García-Santamaría
Frederick Seitz Materials Research Laboratory
1304 West Green St., Urbana, IL 61801 (USA)
[+] Present address: Chemistry Division, Los Alamos National Laboratory, Los Alamos, New Mexico 87545, USA

[**] This material is based upon work supported by the U. S. Army Research Laboratory and the U. S. Army Research Office grant DAAD19-03-1-0227. This work was carried out in part in the Beckman Institute Microscopy Suite, UIUC and the Center for Microanalysis of Materials, UIUC, which is partially supported by the U.S. Department of Energy under grants DE-FG02-07ER46453 and DE-FG02-07ER46471. We gratefully thank Dr. L.-S. Tan (U.S. Air Force Research Laboratory) for providing the two-photon sensitive dyes and Dr. S. A. Rinne (UIUC) for experimental assistance.

dipyromethene (BODIPY) fluorescent dye for imaging that does not show a negative interaction with the TPP process. Unlike other dyes, BODIPY does not quench in the presence of our monomer or quench the TPP reaction, photons at its excitation wavelength are not absorbed by the photoinitiator, and no energy transfer between the dye and the multiphoton photoinitiator or monomer is observed. Consequently, it enables high resolution imaging of the photonic crystal lattice during TPP, facilitating exact placement of features in well-ordered regions of a colloidal crystal.

Reflective and fluorescent imaging are equally effective at the interface of a strongly reflecting substrate such as silicon (Fig. 1a and b). Both images show a line defect in the lower right corner of the image. In the reflectance image, the colloids are bright, while in the fluorescence image the colloids are dark as the dye is contained in the monomer. However, deeper in the crystal, reflectance imaging is not effective due to the strong reflections from the colloidal crystal/substrate interface (Fig. 1c) and the images show a ghost image of the line defect in Figure 1a. This is in clear contrast with the fluorescence image (Fig. 1d), where the line defect from the first layer is no longer visible, showing it is an image artifact in Figure 1c. In addition, the higher resolution of Figure 1d permits observing point defects that are not obvious in the reflectance image. In the case of images corresponding to cross sections perpendicular to the substrate, reflectance imaging (Fig. 1e) also yields optical artifacts where colloids are observed on both sides of the substrate/colloidal crystal interface, even though they only exist on one side of the substrate. Once more, fluorescence imaging (Fig. 1f) provides a more complete and correct image of the crystal, necessary for the positioning of optically functional features.

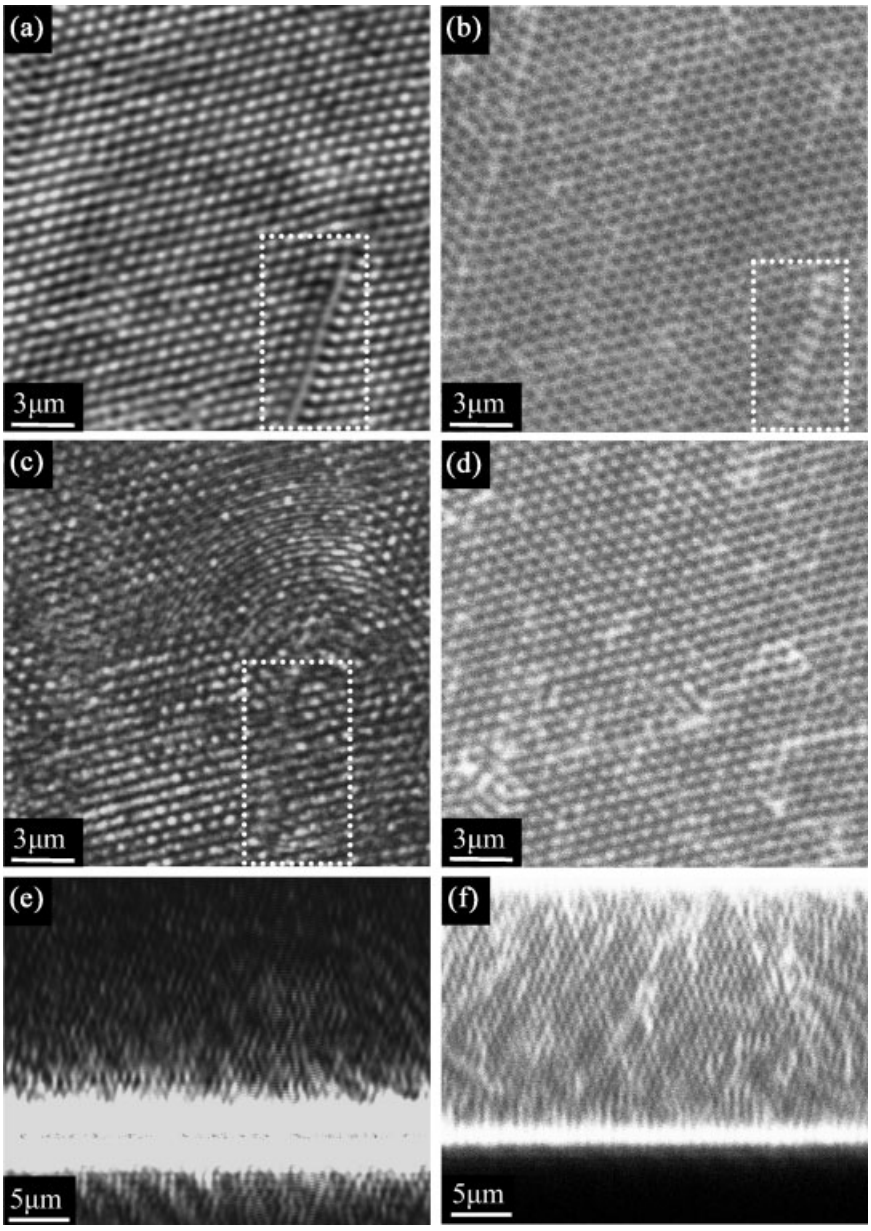

Figure 1. Laser scanning confocal microscopy images. The first layer of colloids on the substrate surface: a) reflectance and b) fluorescence imaging; dotted boxes highlight a line defect. Near the midplane of the colloidal crystal, parallel to the substrate: c) reflectance (dotted box highlights image artifact of line defect) and d) fluorescence imaging. Cross-section: e) reflectance and f) fluorescence imaging. The sphere diameter is 720 nm.

3. Two-Photon Polymerization of Registered Features

TPP features can easily be written through the approximately 17 μm thickness of the colloidal crystal (Fig. 2a–c) using fluorescence imaging (Fig. 2a) for alignment. SEM images (Fig. 2b and c) confirm the high degree of registration seen in the fluorescence image. Notice how the segments of the 60 degree bend feature in Figure 2 follow the orientation of different planes in the colloidal crystal. The SEM images also confirm the ability of fluorescence imaging to detect crystalline defects. The fluorescence image obtained near the top of the crystal (Fig. 2a) shows a bright line defect running between the first positively sloped section of the two features as well as several point defects. The line defect, which propagates up to the top surface of the crystal, is also visible in the SEM image (Fig. 2b).

ADVANCED FUNCTIONAL MATERIALS

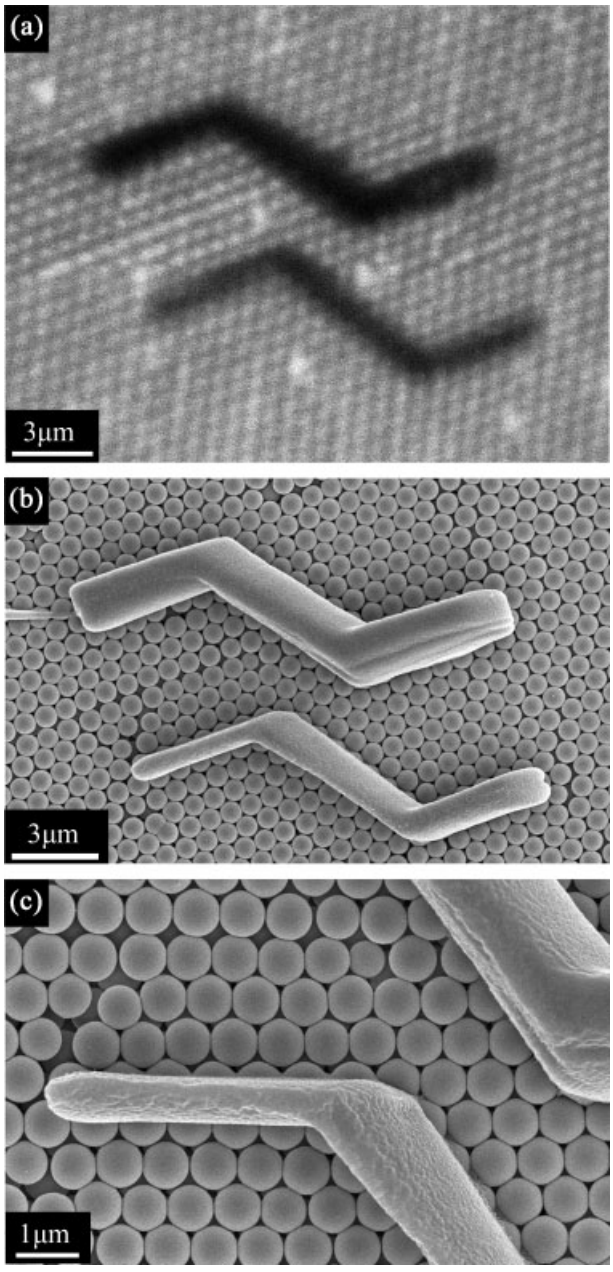

Figure 2. a) Laser scanning fluorescence confocal microscopy image parallel to the substrate of TPP features. The image plane is within the crystal. Defects can be seen near the TPP feature as bright dots or lines. b) SEM image of two TPP features written through the top of the crystal showing the high degree of registration with the colloidal crystal lattice. c) SEM image of the narrower TPP feature highlighting the registration along two crystallographic directions. The sphere diameter is 720 nm.

In addition to straight line features, point features smaller than 500 nm in diameter can also be precisely positioned. The novel possibility of creating point defects (Fig. 3a) with dimensions (approximately 430nm) significantly smaller than the colloid diameter (925 nm) and placing it in a given location, such as the interstice formed by three colloids, highlights the enormous potential of our procedure. A number of designs for optically active structures in PhCs rely on accurate placement

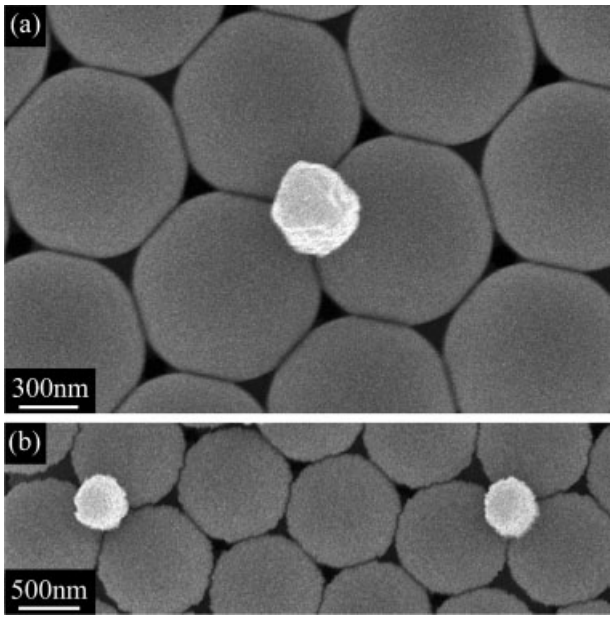

Figure 3. a) SEM image of TPP point feature placed at the interstitial space between three colloids. b) SEM image of two aligned TPP point features each placed at the interstitial space between three colloids. The sphere diameter is 925 nm.

of point defects[14,17–19] including proposed waveguide-cavity resonant structures,[18–21] and related channel drop filters.[22,23] Due to their small size relative to the PhC structure, precise control over the position of point defects is very important. Particularly interesting is the fabrication of low-loss waveguides in colloidal crystals by creating arrays of spherical cavities that allow photons to propagate by tunneling from one to another as suggested by Lousse et al.[12] Figure 3b demonstrates two aligned cavities positioned precisely over the intersticial site in the (111) plane of the crystal, an important first step toward a coupled cavity waveguide.

The examples provided in Figures 2 and 3 show features on the surface of the colloidal crystal but, obviously, it is important to achieve similarly accurate registration for embedded features. Figure 4a presents an embedded polymer feature written with lattice registration near two point defects, which can be observed as bright spots to the right and left of the middle segment of the feature. While unwanted defects may have a negative effect on optical properties, this feature was intentionally written between the unwanted defects to demonstrate the control afforded by our technique. The cross-section normal to the substrate in Figure 4b shows that the feature was written within the bulk of the colloidal crystal, not at an interface.

4. Effect of Feature Placement on Optical Properties

While the crystal is effectively infinite in the x–y plane (parallel to the substrate), this is not the case in the z-direction

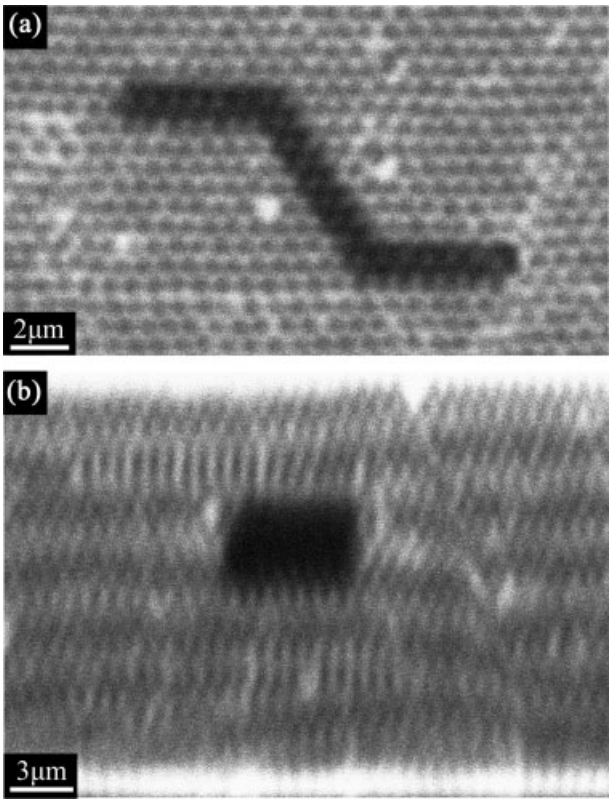

Figure 4. Laser scanning fluorescent confocal microscopy images of a polymer feature embedded near the midplane of the colloidal crystal. a) Section parallel to the substrate. Two point defects in the colloidal crystal are seen as regions of high fluorescent intensity adjacent to the feature. b) Cross-section perpendicular to the substrate. The sphere diameter is 720 nm.

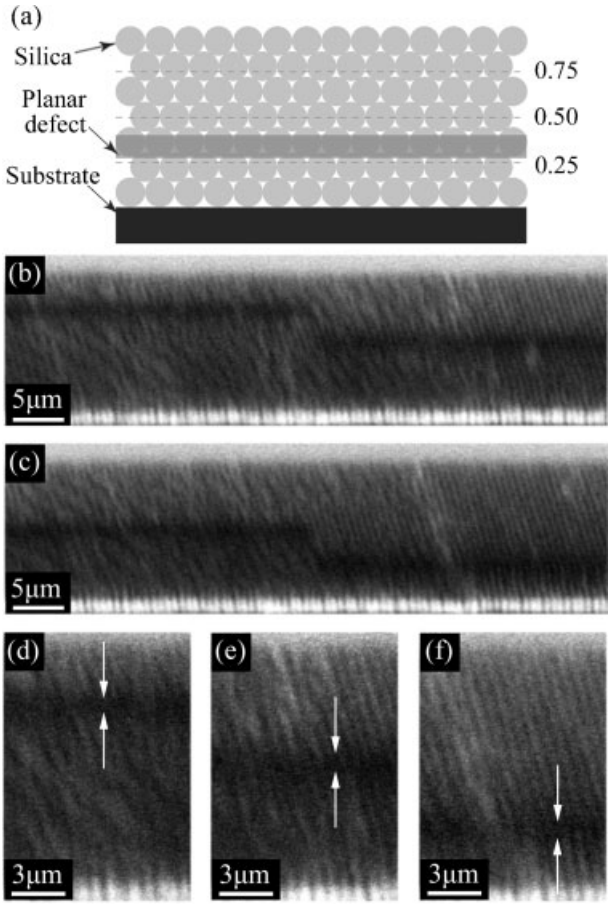

Figure 5. a) Schematic of planar defects written at various locations within a colloidal PhC. b) Defects written at 0.75 and 0.50 according to the schematic in (a). c) Defects written at 0.50 and 0.25 according to the schematic in (a). Magnified images of defects written at 0.75 (d), 0.50 (e), and 0.25 (f) – the white arrows are guides for the eye. The sphere diameter is 720nm.

(normal to the substrate) where it is expected that the position of the defect relative to the substrate, not just its position in the unit cell, will affect the optical properties. This is especially important for cases where light is coupling to an embedded cavity. In this section we show that the precise placement of planar cavities with respect to the crystal thickness has a strong effect on both the spectral width and position of the defect mode.

Planar cavities, approximately 800nm thick, were centered (Fig. 5) at 0.25, 0.50, and 0.75 of the total crystal thickness (measured from the substrate, Fig. 5a) and their optical properties were subsequently investigated. To demonstrate the importance of feature placement in the direction of crystal thickness on the optics of defects, the reflectance was measured for the planar defects and compared to simulations carried out with the Scalar Wave Approximation (SWA) method[24] (Fig. 6). Despite its simplicity, SWA has been successfully utilized in the past to model planar cavities fabricated[25–29] in artificial opals.[30,31] The cavity was modeled as an opal infiltrated with polymer, taking into account the Si substrate effects (both the opal/substrate and substrate/air interfaces). The simulated results matched the experimental data quite well for every case. The defect mode moves from higher to lower energy as the defect is positioned further from the substrate, both in simulation and experiment. The highlighted gray region is the range of frequencies the defect modes occupy for the various defect placements. For this cavity thickness, the defect modes appear at the high energy edge of the gap (the position of the defect within the gray box is a guide to the eye to see where in the bare opal reflectance peak the defect mode appears).

Intuitively, one may expect symmetry in the optical behavior across the plane of the center of the crystal yielding identical reflectance for cavities at, for example, 0.75 and 0.25. This is the case for a crystal surrounded by air on both sides, as seen in Figure 7a, where the contour plots are defect position versus frequency with the colors representing the reflectance intensity. Introducing a substrate in the system breaks the symmetry and cavities placed at 0.75 and 0.25 now demonstrate different behavior (Fig. 7b–d). The refractive index of the substrate dictates the degree of asymmetry of the system; for example, a system with a glass substrate (Fig. 7b) shows a more symmetric behavior than the same case with a silicon substrate (Fig. 7c).

ADVANCED FUNCTIONAL MATERIALS

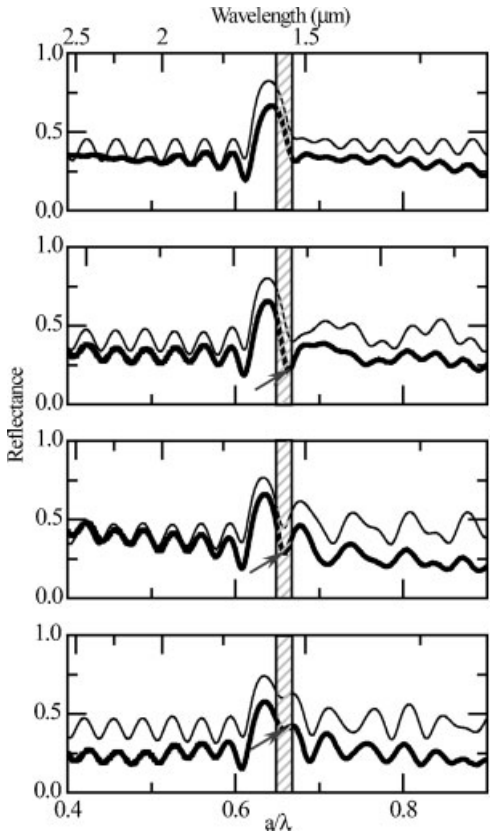

Figure 6. Experimental (thick line) and simulated (thin line) reflectance data for a bare opal (a), opal with a defect at 0.25 of the crystal thickness (b), defect at 0.50 of the crystal thickness (c), and defect at 0.75 of the crystal thickness. The gray box highlights the range of frequencies where the various defect modes appear and the arrows point to the defect mode. The lattice parameter is 1.02 μm.

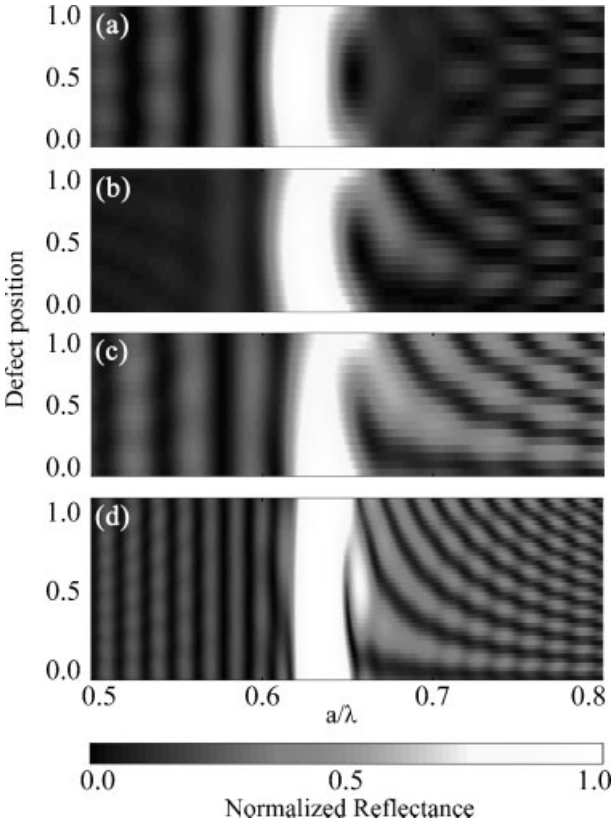

Figure 7. Simulated reflected intensity as a function of defect position and normalized frequency for 17-layer opals with: a) air substrate; b) glass substrate; c) Si substrate. d) A 40-layer opal with Si substrate. All reflectance values are normalized to the maximum and minimum for each simulation for the color bar.

Photonic crystals designed for in the infrared are typically grown on silicon, as would crystals incorporated into an integrated on-chip optical system. Therefore, the position of the defect should be accounted for since it will have an important effect on the spectral position of the resonant modes.

The dependence of the optical behavior on cavity placement is most clearly visualized in Figure 7c. It is clear that the width of the defect modes varies rapidly as the cavity is moved up or down from the center of the crystal. This makes defect placement important if a certain mode bandwidth is required, which is often the case. The case of a 40 layer crystal was also simulated to show the effects of stronger confinement within a cavity (Fig. 7d). There are several effects that become clear with this configuration. The width of the modes greatly decreases since the confinement power increases with the size of the photonic crystal on both sides of the cavity. Also, although the asymmetric behavior of defect placement is still present, it becomes more subtle. The broadening of the defect mode for cavities closer to the substrate is now greatly reduced. With increased crystal thickness, there is increased tolerance for defect placement to achieve the same or a very similar mode width. However, in high quality thin-film opals made of silica spheres, typical thicknesses are around 25 layers or less. Hence, defect placement is particularly important.

5. Conclusions

We have demonstrated a method to precisely embed engineered defects in a photonic crystal, not only with respect to the substrate, but also with respect to other features such as the building blocks of the lattice or crystalline defects (in order to avoid them). Fluorescence imaging combined with two-photon polymerization provides substantial advantages over previous techniques and allows imaging through the thickness parallel to the substrate and imaging of the entire cross-section perpendicular to the substrate. Now it should be possible to fabricate low-loss waveguides that are made of spherical cavities in colloidal crystals. We have shown that the optical response of planar cavities can be greatly affected by not only the in-plane alignment of the cavities but also their position relative to the surface of the PhC. The ability of light

to couple to embedded defects as well as the spectral width and position of the defect modes depend on the location of the defect within the crystal thickness, making precise control over defect placement essential. The techniques demonstrated here may enable the fabrication of numerous 3D photonic devices that require specific feature placement within the photonic structure.

6. Experimental

Colloidal crystals were prepared from 730 and 925 nm diameter silica particles using a vertical evaporation technique similar to that described elsewhere [15]. Opals were filled with 6 nm of aluminum oxide grown conformally using atomic layer deposition (ALD, Cambridge Nanotech Savannah [4]). Colloidal crystals were characterized by FTIR spectroscopy using a Bruker Hyperion microscope coupled into a Bruker Vertex 70 FTIR spectrometer equipped with a 4x, 0.1 NA objective and a collection area of 187.5 μm achieved using a spatial aperture. Crystal quality was evaluated by measuring the low energy reflectance peak caused by reflections from opal layers in the (111) direction in several locations on the crystal. The crystals used in this study had reflectance values ranging from 63–81% for 15 to 22 layers.

The TPP solution was composed of trimethylolpropane triacrylate (TMPTA) monomer (Sigma–Aldrich) with inhibitor; 0.1 wt % AF-350 photoinitiator (tris[4-(7-benzothiazol-2-yl-9,9-diethylfluoren-2-yl)phenylamine) donated by the Air Force Research Laboratory [32] and 10 μM Invitrogen BODIPY 630/650-X, SE (6-(((4,4-difluoro-5-(2-thienyl)-4-bora-3a,4a-diaza-*s*-indacene-3-yl)styryloxy)acetyl)aminohexanoic acid, succinimidyl ester). The BODIPY dye has an absorption maximum of 625 nm and an emission maximum of 640 nm; neither wavelength causes single-photon excitation of the photoinitiator.

Confocal imaging and TPP were performed on a laser scanning confocal microscope (Leica DMIRBE with an SP2 scanhead). Reflectance and fluorescence imaging was performed with a 633 nm HeNe laser. Spatially defined TPP was achieved through our published procedure [9,10]. Point defects were written using software defined bleach points. Samples were mounted with the colloidal crystal facing a coverslip; TPP is performed through the coverslip. Imaging and ROI alignment were performed using a beam expander to fill the back aperture of the objective to improve image quality in the microscope. TPP was performed with the beam expander removed; rotational alignment was unaffected by the change because the scan field does not rotate. The absolute position of the ROI in the *x*–*y* plane (parallel to the substrate) varies with the presence of the beam expander and is compensated for prior to writing the feature. The position of the ROI and the resultant polymer feature are systematically not coincident in the direction of the crystal thickness; the ROI is positioned offset from the desired feature location to compensate. After TPP samples were rinsed in ethanol to remove excess monomer and dried in air. Scanning electron microscopy (SEM) samples were gold-palladium-coated prior to imaging; the micrographs were taken using a Hitachi S-4700 SEM.

The parameters for the SWA simulations are: $n_{\text{silica}} = 1.44$, $n_{\text{polymer}} = 1.55$, $n_{\text{air}} = 1$; 12 layers above and 5 below (0.25 cavity), 8 layers above and 9 below (0.5 cavity) and 4 layers above 13 below (0.75 cavity). Layers above and below do not equal exact crystal thickness fractions because the SWA code requires the crystal thicknesses be integer numbers of layers; the thickness fractions are within a few percent and the fits are good. In order to fit the data the SWA simulations required 17 total layers of crystal (sum of layers above and below the cavity) for the cases of the defect and 18 layers for the bare opal (without a cavity). This can be understood from the fact that the thickness of the total system for the bare opal is simply the thickness of the crystal layers, whereas for the cases with the cavity it also includes the thickness of the defect. For all defect placements the defect thickness was approximately one layer thickness (0.56a for the 0.25 defect and 0.61a for the 0.5 and 0.75 defects, a reasonable difference of approximately 64 nm in our experimental system) making the total thickness of the bare opal and opal with planar defect approximately the same, just as they are experimentally. The spheres are interpenetrated to model the experimental system where a thin ALD layer is grown on the spheres to yield interpenetration. The Fourier component of the dielectric constant for the 111 reciprocal lattice vector is numerically calculated taking into account the sphere interpenetration. This is more accurate than using the analytical Rayleigh–Gans expression [24] which assumes the building blocks of the lattice are perfectly spherical.

Received: February 07, 2008

[1] E. Yablonovitch, *Phys. Rev. Lett.* **1987**, *58*, 2059.
[2] S. John, *Phys. Rev. Lett.* **1987**, *58*, 2486.
[3] J. D. Joannopoulos, P. R. Villeneuve, S. Fan, *Nature* **1997**, *386*, 143.
[4] S. A. Rinne, F. Garcia-Santamaria, P. V. Braun, *Nat. Photon.* **2008**, *2*, 52.
[5] S. John, T. Quang, *Phys. Rev. Lett.* **1997**, *78*, 1888.
[6] S.-Y. Lin, E. Chow, V. Hietala, P. R. Villeneuve, J. D. Joannopoulos, *Science* **1998**, *282*, 274.
[7] S. Noda, K. Tomoda, N. Yamamoto, A. Chutinan, *Science* **2000**, *289*, 604.
[8] A. Mekis, J. C. Chen, I. Kurland, S. Fan, P. R. Villeneuve, J. D. Joannopoulos, *Phys. Rev. Lett.* **1996**, *77*, 3787.
[9] W. Lee, S. A. Pruzinsky, P. V. Braun, *Adv. Mater.* **2002**, *14*, 271.
[10] S. A. Pruzinsky, P. V. Braun, *Adv. Funct. Mater.* **2005**, *15*, 1995.
[11] M. Qi, E. Lidorikis, P. T. Rakich, S. G. Johnson, J. D. Joannopoulos, E. P. Ippen, H. I. Smith, *Nature* **2004**, *429*, 538.
[12] V. Lousse, S. Fan, *Opt. Express* **2006**, *14*, 868.
[13] M. Okano, A. Chutinan, S. Noda, *Phys. Rev. B* **2002**, *66*, 165211-1.
[14] B. Li, X. Cai, Y. Zhang, *Appl. Phys. Lett.* **2006**, *89*, 031103-1.
[15] P. Jiang, J. F. Bertone, K. S. Hwang, V. L. Colvin, *Chem. Mater.* **1999**, *11*, 2132.
[16] B. Griesebock, M. Egen, R. Zentel, *Chem. Mater.* **2002**, *14*, 4023.
[17] Y. Akahane, M. Mochizuki, T. Asano, Y. Tanaka, S. Noda, *Appl. Phys. Lett.* **2003**, *82*, 1341.
[18] M. F. Yanik, S. Fan, M. Soljacic, *Appl. Phys. Lett.* **2003**, *83*, 2739.
[19] M. Soljacic, C. Luo, J. D. Joannopoulos, S. Fan, *Opt. Lett.* **2003**, *28*, 637.
[20] M. Okano, S. Kako, S. Noda, *Phys. Rev. B* **2003**, *68*, 235110-1.
[21] P. Kohli, C. Christensen, J. Muehlmeier, R. Biswas, G. Tuttle, K.-M. Ho, *Appl. Phys. Lett.* **2006**, *89*, 231103-1.
[22] S. Fan, P. R. Villeneuve, J. D. Joannopoulos, *Phys. Rev. Lett.* **1998**, *80*, 960.
[23] S. Fan, P. R. Villeneuve, J. D. Joannopoulos, H. A. Haus, *Opt. Express* **1998**, *3*, 4.
[24] K. W. K. Shung, Y. C. Tsai, *Phys. Rev. B* **1993**, *48*, 11265.
[25] F. Fleischhaker, A. C. Arsenault, J. Schmidtke, R. Zentel, G. A. Ozin, *Chem. Mater.* **2006**, *18*, 5640.
[26] Z. Yuxia, K. Wostyn, G. de Schaetzen, K. Clays, L. Hellemans, A. Persoons, M. Szekeres, R. A. Schoonheydt, *Appl. Phys. Lett.* **2003**, *82*, 3764.
[27] R. Pozas, A. Mihi, M. Ocana, H. Miguez, *Adv. Mater.* **2006**, *18*, 1183.
[28] E. Palacios-Lidon, J. F. Galisteo-Lopez, B. H. Juarez, C. Lopez, *Adv. Mater.* **2004**, *16*, 341.

ADVANCED FUNCTIONAL MATERIALS

[29] N. Tetreault, A. Mihi, H. Miguez, I. Rodriguez, G. A. Ozin, F. Meseguer, V. Kitaev, *Adv. Mater.* **2004**, *16*, 346.
[30] J. F. Galisteo-Lopez, M. Galli, L. C. Andreani, A. Mihi, R. Pozas, M. Ocana, H. Miguez, *Appl. Phys. Lett.* **2007**, *90*, 101113.
[31] A. Mihi, H. Miguez, I. Rodriguez, S. Rubio, F. Meseguer, *Phys. Rev. B* **2005**, *71*, 125131.
[32] G. S. He, J. Swiatkiewicz, Y. Jiang, P. N. Prasad, B. A. Reinhardt, L.-S. Tan, R. Kannan, *J. Phys. Chem. A* **2000**, *104*, 4805.